Segregation and ordering at the (1×2) reconstructed $Pt_{80}Fe_{20}(110)$ surface determined by low-energy electron diffraction

R. Baudoing-Savois, Y. Gauthier, and W. Moritz*
Laboratoire de Spectrométrie Physique, Université Joseph Fourier, Boîte Postale 87, 38402 Saint-Martin d'Hères, France
(Received 15 January 1991; revised manuscript received 28 May 1991)

The surface of an ordered $Pt_{80}Fe_{20}(110)$ crystal exhibits (1×2) and (1×3) reconstructions depending on the annealing treatment after ion bombardment. The (1×3) structure occurs after annealing in the range 750 to 900 K. Annealing above 1000 K leads to the (1×2) structure, which is, from the present result, unambiguously attributed to the same geometrical reconstruction as Pt(110) but with smaller relaxation amplitudes: a detailed low-energy electron-diffraction analysis concludes to a missing-row structure with row pairing in layers 2 and 4 accompanied by a buckling in layers 3 and 5. The top layer spacing is contracted by 13%, and further relaxations are detectable down to the fifth layer. The specific diffraction spots associated with the bulk chemical ordering along the dense [$\bar{1}$10] rows are very weak: The $I(V)$ analysis shows that this chemical ordering is absent in the outermost "visible" rows but gradually recovers over five to six layers deep. General Pt enrichment is found in the surface "visible" rows (in layers 1–3), but segregation and order yield a subtle redistribution of Pt and Fe atoms in deeper rows: For example, in layer 2, the visible row is Pt rich, whereas the other row (buried under layer 1) is enriched with Fe. Because of the many parameters considered, a fit procedure was applied to a large data basis to solve the structure; the results were confirmed and illustrated subsequently by a standard $I(V)$ analysis for the most relevant parameters. The final r factors are $R_{DE}=0.36$, $R_P=0.34$, and $R_{ZJ}=0.14$ for two beam sets at normal and oblique incidence consisting of 26 and 21 beams, respectively.

I. INTRODUCTION

(1×2) reconstructions are known for the (110) faces of fcc metals like Pt,[1] Au,[2] and Ir,[3] and it is now well established that the correct picture is a missing row model including atomic displacements in subsurface layers: the main features are a row pairing in layer 2 and a buckling in layer 3, accompanied by a strong contraction of the first interlayer spacing. In addition to the (1×2) reconstruction, (1×3) reconstructions have also been reported for these three metals.[4–6] Recent work using low-energy electron diffraction[1] (LEED) has emphasized the importance of atomic displacements in subsurface layers to reach a good agreement between experimental and theoretical $I(V)$ spectra.

In addition to reconstruction problems, catalytic properties of Pt-M (M a 3d transition metal) surfaces are of much interest. PtNi alloys have shown marked orientation effects with respect to reactivity and selectivity, in connection with segregation reversal:[7] Pt segregates to enrich the top layer of $Pt_xNi_{1-x}(111)$,[8] whereas Ni enrichment occurs for $Pt_xNi_{1-x}(110)$.[9,10] The PtFe system is also of great interest since 4–5-nm aggregates, for instance, exhibit enhanced catalytic properties by an order of magnitude in a narrow range of composition (80±15 at. % Pt) for a particular reaction.[11] In a recent work,[12] we have found that on $Pt_{80}Fe_{20}(111)$, Pt segregation occurs, giving rise to two different Pt catalytic sites at different heights: such a particular atomic arrangement might be at the origin of the enhanced activity. It is thus important to know what happens to the other low index planes of this $Pt_{80}Fe_{20}$ alloy, and more specially the open face for which an even better activity was observed.[13] The present study reports on the (110) face, adding complementary information to our results on the (111) face.

II. EXPERIMENTAL DETAILS

The experiments were carried out in an ultrahigh vacuum system equipped with hemispherical optics (glass screen and grids) used for LEED and Auger electron spectroscopy (AES) in the retarding field mode. The electron gun, movable from normal to grazing incidence, can work in a wide energy range, from 10 eV to 2–3 keV. The $I(V)$ spectra are measured by means of a spotphotometer mounted on a two-circle goniometer allowing to collect the intensities of the beams diffracted in any direction, in the whole half space above the crystal. Three pairs of large Helmholtz coils minimize the residual magnetic fields to insure a perfect alignment. The crystal is fixed on a sample holder which can be rotated 360° around the normal to the surface. The incidence (polar and azimuthal angles) can be set with a precision of 0.1° while the residual tilt could be reduced below 0.1° by means of the specular reflection.

A. Sample

The crystal (about 7 mm in diameter and 2-mm thick) was initially cut from a monocrystaline rod. Its surface was polished with diamond powder (down to 1 μm grain size) and the final surface was not more than 10′ off the true crystallographic planes.

At high temperature, Pt_xFe_{1-x} has a disordered phase[14] (γ phase). At room temperature, in the range 65

to 82 at. % Pt, this alloy crystallizes with a γ_3 structure (Fig. 1) whereas for larger Pt content a γ phase is known. In a previous study[12] of the $Pt_{80}Fe_{20}(111)$ surface, the rod (from which the sample was cut) was proved to be in the ordered state, with a Au_3Cu-like structure. The present sample was found mainly in the γ_3 phase with the possible occurrence of a small γ phase part. The bulk ordering is not detectable by LEED because only 10–15 layers are probed by the electron beam. Deviations from bulk ordering could extend over that depth. In the *I-V* analysis presented below, compositional and geometrical parameters within the top five layers were considered and the layers below were considered either ordered or disordered. A preference has been found for ordered layers below the fifth layer. This is in agreement with the x rays results assuming that the distorted surface region includes only a few layers in metals and alloys. We originally intended to study first the disordered phase but, most probably because of the high order-disorder transition temperature, it was not possible to freeze this state.

Figure 1 shows the bulk structure of an ideal Pt_3Fe ordered crystal, the Pt (Fe) atoms being perfectly situated on the "Pt sublattice" ("Fe sublattice"). The Pt concentration measured in several places by means of x-ray fluorescence was 80 ± 0.5 at % Pt corresponding to a lattice constant $a=3.90$ Å (Ref. 15) and a bulk interlayer spacing $d_{\text{bulk}}=1.379$ Å. The excess platinum is assumed to be uniformly distributed at the Fe sites, which thus contain a mixture of $\frac{4}{5}$ Fe plus $\frac{1}{5}$ Pt atoms.

B. Mesh definition

In the $[\bar{1}10]$ direction normal to the surface, the crystal exhibits a stacking sequence of two different layers with 60 and 100 at. % Pt so that a truncated bulk can end, on the vacuum side, with two possibilities. This is illustrated in Fig. 2 which displays a top view of an ideal $Pt_{80}Fe_{20}(110)$ surface with the two possible terminations and, anticipating the result, with a missing row reconstruction in the top layer. The two terminations can be distinguished irrespective of the actual geometry and composition of the surface layers.

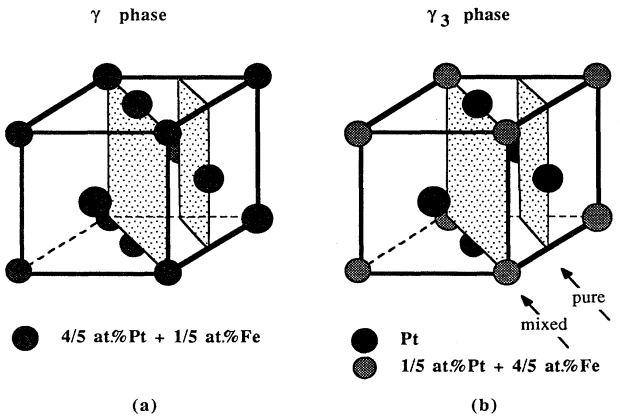

FIG. 1. Structure of the γ and γ_3 phases of $Pt_{80}Fe_{20}$: stacking of pure and mixed (110) planes in the γ_3 phase.

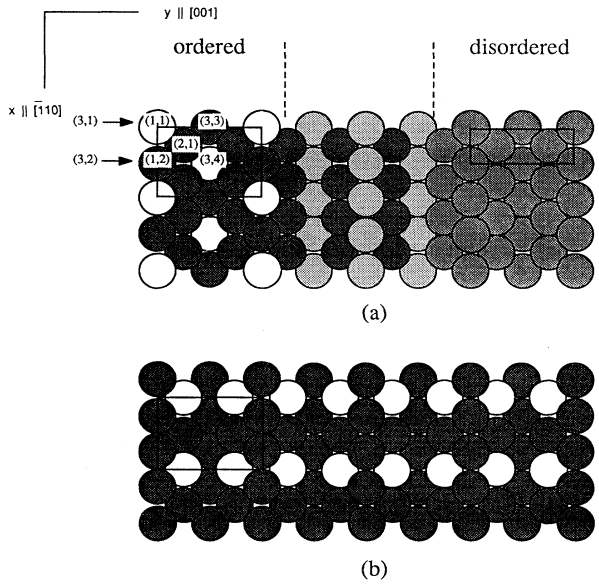

FIG. 2. $Pt_{80}Fe_{20}(110)$ top view showing the first three layers of a truncated bulk with missing rows in the top layer. Two terminations are possible. (a) A Sequence of layers containing 60,100,60, ... at. % Pt, respectively. Left, ordered γ_3 phase; right, disordered γ phase; central part, intermediate situation where chemical ordering along the $[\bar{1}10]$ rows is not considered. This latter picture is the one used for the calculations of Sec. V C. (b) Same as (a), with a sequence 100%-60%-100%. The site labels (layer and atom number) are used in the tables below.

Because of the chemical order, the truncated bulk structure has a unit cell twice as large than that of the γ phase in the $[\bar{1}10]$ direction and could be described as a (2×1) superstructure of the γ phase. Instead it is much more natural to take this bigger unit cell as the bulk 2D unit mesh which will then be referred to as a (1×1) structure in the present work. The reconstructed surface is then referred to as a (1×2) superstructure.

C. LEED pattern

After introduction in the chamber, we performed several preliminary 10-min anneals at 1250 K to recrystallize the surface region perturbed by mechanical polishing. Subsequently, a clean surface was obtained with repeated cycles of Ar ion bombardment and anneals in the range 750 to 1200 K. As evidenced by Auger spectra, no traces of contaminants were detected in the limit of the sensitivity.

Two different LEED superstructures are observed which, in our convention, are described as (1×2) and (1×3). Both superstructures were produced similarly by annealing the bombarded surface: (1×3) in the temperature range from 750 to 900 K; and (1×2) above 1000 K as illustrated in Fig. 3(a). The annealing time (typically 5 min) influences neither the intensity nor the AES signals.

The same (1×2) superstructure [same AES spectra, same $I(V)$ curves] could also be obtained starting from the (1×3) structure and the subsequent anneal at 1000 K. Cooled down to room temperature these structures remain stable for hours of measurements in the low 10^{-10} torr pressure range.

At intermediate stages, the (1×2) and (1×3) structures coexisted and at certain conditions, streaks elongated in the [001] direction were visible as shown in Fig. 3(a). Background features are quite common with binary alloys and are generally attributed to partial (dis)order in the distribution of both species in the first few layers in connection with segregation and with the lack of stoichiometry. In this case, streaks in the [001] direction correspond to partial correlation between dense rows or disordered reconstruction and not to chemical disorder along these dense rows. The streaks could, for instance, be assigned to steps on the surface because the missing row reconstruction requires a mass transport in the top layer. Streaking could not be completely removed even after long-time annealing but the data used in the present study correspond to a LEED diagram in which little streaking was observed. The density and distribution of steps has not been analyzed in the present work. The fact that only little diffuse intensity was observed indicates that only a small fraction of the surface is disordered. This should be of little influence on the I/V curves for the sharp reflections.

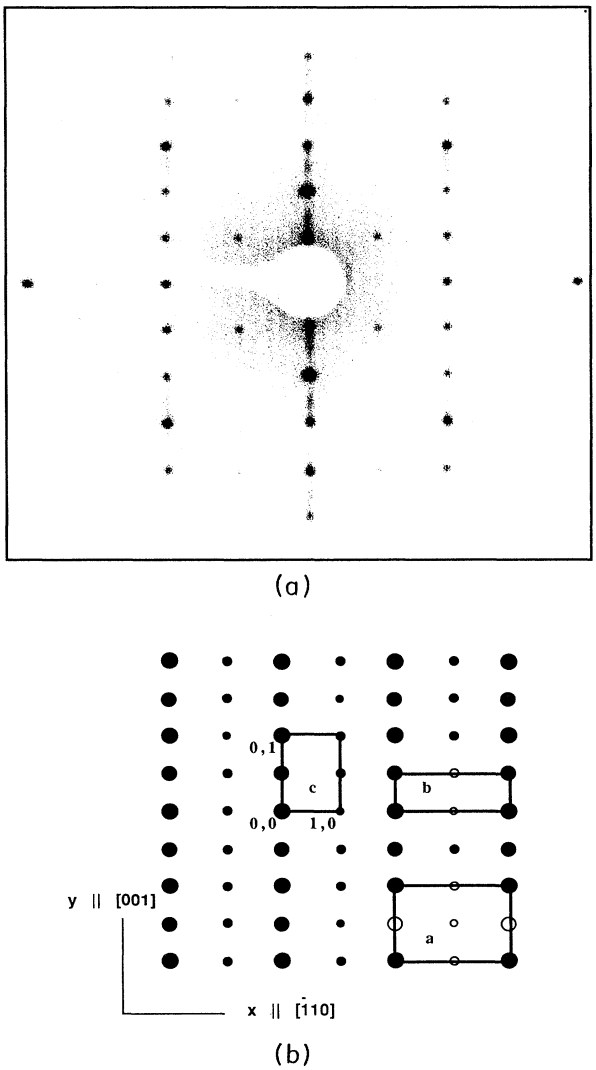

FIG. 3. $Pt_{80}Fe_{20}(110)(1\times2)$ (a) normal incidence LEED pattern at 125 eV. Note the weak intensity of the (h_0,k) spots compared to the other ones. (b) Schematic LEED pattern. The spot sizes are roughly proportional to their average intensity: *a*, unreconstructed bulk unit cell of the fcc lattice (γ phase); *b*, (1×2) reconstruction unit cell for a disordered bulk (γ phase); and *c*, (1×1) unit cell for an ordered bulk (γ_3 phase).

A schematic view of the LEED pattern is shown in Fig. 3(b). The unit cell *c*, corresponding to the γ_3 phase as shown in Figs. 1 and 2, is doubled in the $[\bar{1}10]$ direction compared to that of a pure unreconstructed (110) fcc face (unit cell *a*). With the convention adopted in the preceding section, all beams labeled (h,k) should occur if the chemical ordering in the $[\bar{1}10]$ direction is maintained while in the case of a disordered bulk, only those beams (h,k) with h even can appear (unit cell *b*). The $(h,k/2)$ beams are due to the missing row reconstruction. In the following (h_e,k) and (h_0,k) denote beams with even and odd h indices, respectively.

D. Data

The reproducibility of the *I-V* curves was checked by repeated measurements after new cleaning cycles. Special care was taken to adjust the incidence by controlling the intensities of symmetrically equivalent beams. The intensities were normalized for constant incident current after background substraction.

The $I(V)$ curves were collected by means of a computer controlled device in steps of 1 eV in the energy range 30–280 eV in three different incidence conditions: 26 beams were recorded at normal incidence and 21 beams at oblique incidence (20° off normal) in the (110) and (001) crystal planes. Only the first two data sets were included in the present analysis.

III. STRUCTURE MODELS

The clean surface exhibits a (1×2) pattern where the (h_e,k) beams are very intense, in contrast with *systematically weak* (h_0,k) *beams*. The latter become visible at high energy, above approximately 100 eV with average intensities only about 1% to 10% that of the other spots as illustrated in Fig. 3. In other words, the pattern resembles that of Pt(110)-(1×2) [unit cell *b* in Fig. 3(b)] with additional weak (h_0,k) beams. The same remarks hold for the (1×3) reconstruction with very weak (h_0,k) spots appearing on a (1×3) pattern.

The (1×2) $I(V)$ curves of the h=even beams closely resemble the corresponding $I(V)$ curves of the Pt(110)-(1×2) structure[16] as shown in Fig. 4. On the contrary, large differences are clearly seen between the (1×3) $I(V)$ spectra of the alloy and those of Pt(110).[1] Another no-

ticeable difference is the sequence in which both reconstructions occur: the (1×2) structure appears after high-temperature annealing of the alloy crystal while at the pure metal surface, the (1×2) appears after low-temperature annealing. The (1×3), presently under analysis, will be reported in a forthcoming article and, in the following, we focus our attention on the (1×2) structure only.

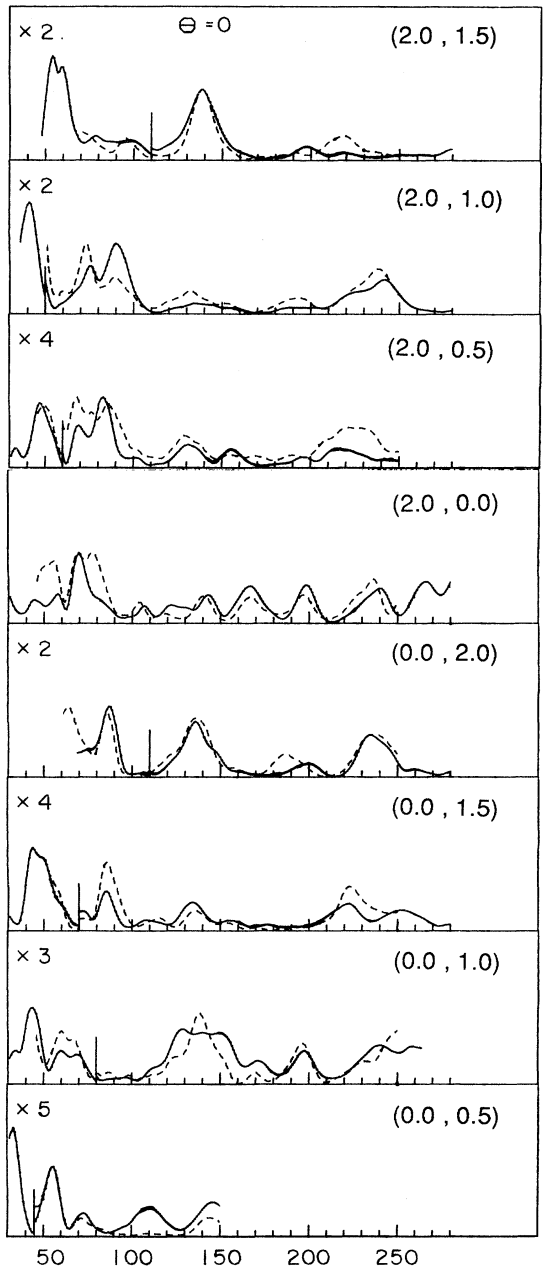

FIG. 4. Experimental spectra at normal incidence. $Pt_{80}Fe_{20}(110)$ (——) compared to pure Pt(110) (Ref. 16) (— — —). From the similarities it can be concluded that the geometry of the surface region of the alloy is approximately the same as that of the metal, i.e., the missing row model and distortions in deeper layers.

The striking similarity in the $I(V)$ curves of the Pt(110) and $Pt_{80}Fe_{20}(110)$ (1×2) surfaces (Fig. 4), coupled with the fact that they both have a fcc structure and the same lattice constant within 0.5% (3.90 against 3.92 Å), leads to a *probable geometric model which should be very similar.* We therefore chose the missing row model with the geometrical parameters of the pure Pt(110)-(1×2) structure as a start model. Indeed, it has been shown[1] for the pure Pt(110)-(1×2) surface that all other models give substantially different $I(V)$ curves and it can be safely assumed that this would also be the case for the alloy surface; however, as explained below, calculations did prove that all the other top rows *were actually missing* (see below, Sec. V C). Models other than the missing row model have thus not been considered in the present analysis.

IV. CALCULATION PROCEDURE

A. Phase shifts and the ATA approximation

The nonstructural parameters used throughout the analysis were the same as used in a previous calculation for $Pt_{80}Fe_{20}(111)$.[12] Pt and Fe phase shifts were calculated from a crystal potential of pure metal obtained from a superposition of atomic potentials. For Pt, spin-averaged phase shifts were used and up to ten phase shifts were included in the calculations. For Fe a nonrelativistic potential was used. Thermal vibrations were considered by bulk Debye temperatures for all layers, $\Theta_{D,\mathrm{Pt}}=240$ K and $\Theta_{D,\mathrm{Fe}}=437$ K. A separate run was performed with a variable surface Debye temperature but it resulted in no improvement.

Variable concentrations of Pt and Fe on different lattice sites were treated in the average t-matrix approximation (ATA). The atomic scattering factors for a mixture of two components at temperature T are given by

$$t_l(C_A,T)=C_A e^{i\delta_l^A}(T)\sin\delta_l^A(T) + (1-C_A)e^{i\delta_l^B}(T)\sin\delta_l^B(T)\ , \quad (1)$$

where δ_l are the phase shifts. The concentration C_A of element A depending on layer and lattice sites has been taken as a variable parameter in the analysis. This approximation has been successfully used in a number of LEED analyses of alloy surfaces [PtNi (Refs. 7–10, 17 and 18) and PtFe (Ref. 12)] and substoichiometric refractory compounds such as $VN_{0.89}$ (Ref. 19) for which excellent agreement is reached. In addition it has been proven excellent compared with coherent potential approximation (CPA) calculations.[20]

B. Fit procedure and discrete sampling

In the analysis the least-squares optimization procedure described earlier[21,22] has been applied. This procedure allows the rapid determination of a large number of parameters which would have not been possible with the conventional grid search method. The quantity which is minimized in the optimization procedure is an r factor R_{DE} defined for discrete energies:

$$R_{\mathrm{DE}} = \sum_g W_g \frac{\sum_i |I_i^{\mathrm{expt}} - C_g I_i^{\mathrm{theor}}|}{\sum_i |I_i^{\mathrm{expt}}|} , \quad (2)$$

where

$$C_g = \sum_i I_i^{\mathrm{expt}} / \sum_i I_i^{\mathrm{theor}}$$

is a scale factor for each beam and $W_g = n_g / \sum_g n_g$ is a weight factor to take account of the different number of data points per beam.

It has been extensively tested previously that this r factor is quite applicable for structure analysis and does not require the calculation of $I(V)$ spectra on a fine energy grid, thus minimizing the calculational effort. The main advantage of the above-defined r factor is that it allows us to apply standard optimization procedures. The method applied here is a combination of a gradient method and the expansion method[23] which takes advantage of both methods, namely, rapid convergence far away from the minimum, like the gradient method, and numerical stability near the minimum.

Throughout the calculations, an energy grid of 15 eV was used. Discrete sampling of LEED data [the $I(g)$ method proposed by Clarke[24]] has already been applied successfully using much larger steps in the case of Ni(110).[25] The method applied here differs from that proposed by Clarke by comparing relative intensities of each beam separately instead of comparing the relative intensities of all beams at the same energy. In a previous investigation, a number of 10–15 points per beam corresponding to a step width of 15 eV has been found to be sufficient. To display the full $I(V)$ spectra and to demonstrate the reliability of the result, for the most important parameters, a grid search was applied, using a small step width of 3 eV on the energy scale. In these cases, three r factors commonly in use have been calculated, namely, Zanazzi and Jona's r factor[26] (R_{ZJ}), Pendry's r factor[27] (R_P), and metric distances.[28]

C. Multiple scattering calculations

LEED intensity calculations were performed applying the layer doubling method for interlayer multiple scattering, and the symmetrized matrix method for intralayer multiple scattering. To avoid spurious effects due to lack of convergence in the presence of heavy atoms like Pt, all layers with a normal distance smaller than 1.2 Å were taken as composite layers where multiple scattering was calculated in angular momentum space. The size of the matrices was reduced by using symmetry adapted functions.[29]

The real and imaginary part of the inner potential were taken to be energy dependent: the real part was approximated by $V_0(E) = -2.4 + 80/(E+20)^{1/2}$ given E in eV, which agrees with previously used data[12] in the energy range 60–300 eV. The imaginary part, the absorption potential, also variable with energy, is taken as $V_i(E) = 0.85(E^{1/3})$.

Two sets of experimental spectra were considered in the analysis covering a very wide overall energy range. The normal incidence set consisted of 26 beams for an overall energy range of about 5000 eV and included 21 (h_e,k) beams (3910 eV). Because of the limited range in which they have noticeable intensities, only five extra beams (h_0,k) (total energy range 1040 eV) could be added to the data set. The set at oblique incidence in the $[\bar{1}10]$ direction contained 21 beams for a total range of 4640 eV; only (h_e,k) beams were measured at oblique incidence.

With 15-eV steps, from 65 to 275 eV, this corresponded to 249 points at normal incidence and 293 at oblique incidence, a number which is highly sufficient to determine *16 independent parameters* in the first part of the analysis using the 21 (h_e,k) beams. During the fit procedure (see below), the main part of the analysis was based on the data at normal incidence. In a later step, 71 extra data points from the five (h_0,k) beams were added to determine nine additional parameters connected to chemical ordering.

V. STRUCTURE ANALYSIS

A. Strategy

We have mentioned above that the average intensity of the (h_0k) spots is very weak compared to that of the other beams. This indicates that the bulk chemical ordering is probably not continued up to the top layer, and further that possible geometrical relaxations related to the chemical order should be small. In the $I(V)$ analysis these qualitative considerations were nicely confirmed.

Neglecting those weak (h_0,k) beams should not spoil the analysis of the (1×2) periodicity due to surface reconstruction. We have shown previously, in the case of the $Pt_{80}Fe_{20}(111)$-(2×2) surface, that the γ phase beams alone can be used to determine *the average composition* of the layers as well as *geometrical parameters* along the normal to the surface. In the kinematic theory of diffraction this procedure would be completely correct. The result, found also in the present analysis, that the superstructure due to chemical ordering practically does not influence the average composition determined from the (1×1) spots, underlines the validity of the ATA approximation.

For a disordered alloy in the γ phase, segregation effects can build up a composition profile versus depth at the surface: in this case, it is sufficient to discuss the partial chemical ordering along the normal to the surface. For an ordered alloy in the γ_3 phase, the discussion must consider the lateral order due to the bulk structure and the influence of the reconstruction of the surface.

In the case of $Pt_{80}Fe_{20}(110)$ under study, the substrate is a pile of doublets of two layers with average Pt concentrations of 100 and 60 at. %, along the z axis. The mixed planes (60 at. % Pt) consist of dense mixed rows, along the $[\bar{1}10]$ direction (x axis), built up with alternating Pt sites and Fe rich sites. Close to the surface, the composition in the rows may differ from that in the bulk rows and the composition profile in the [001] direction (y axis) normal to the rows can change both because of reconstruction (missing row) and segregation.

In the structure determination, several levels of complexity can be retained: a totally ordered alloy, with ordering in three directions [Fig. 2(a), left], or a substitutional alloy with different layer compositions as displayed in Fig. 2(a), right. There is a third possibility [Fig. 2(a), middle] which consists in keeping chemical ordering in the z and y direction but neglecting it in the x direction: the species Pt and Fe are then assumed to be randomly distributed within the rows and replaced by average atoms. As a result, (h_0,k) beams should vanish, approaching the present case where they are weak.

Owing to the complexity of the problem discussed above, it clearly appears that the relevant physical parameters are "average row concentration" in a given layer or "site concentration" in a given row of a given layer rather than "average layer concentration" as previously used for substitutionally disordered alloy surfaces: indeed, on this surface, molecules see isolated rows and (111) facets.

Optimization was made first, neglecting the chemical ordering along the dense rows. We considered only the (1×2) periodicity, limiting the data basis to the 21 (h_e,k) beams in order to determine the average row concentrations plus the geometrical parameters related to the missing row reconstruction. In a second stage, we introduced the periodicity due to chemical order in the $[\bar{1}10]$ direction using the five extra (h_0,k) beams at normal incidence and keeping the other parameters at the predetermined optimum values. In a final step, all beams were considered at a time to ensure that the true minimum in the parameter space was found.

As a final and important check, it was proven that the data at oblique incidence produced the same minimum within the error bars. This proves two things: (i) the normal incidence data set was large enough to determine the many parameters needed, and (ii) the quality of the data is excellent and has led to a very stable picture. This is mainly due to using a LEED goniometer which allows high-precision alignment of the crystal and of the angular setting.

B. Bulk stacking and top layer

Including the bulk chemical ordering or not has important implications in the analysis. Due to the bulk stacking of inequivalent layers coexisting with the missing row model, two geometries are allowed as illustrated in Figs. 2(a) and 2(b). Additional models are obtained by shifting the top two layers by half the unit vector in the $[\bar{1}10]$ direction, which amounts to a stacking fault. Along this direction, atoms (1,1) and (1,2)—the labeling of atoms is described in Fig. 2(a)—are symmetrically inequivalent, allowing different heights and/or occupation factors.

In fact, one bulk stacking sequence, that of Fig. 2(b), was rapidly discarded. Consequently, the missing rows are, a priori, perfectly localized with respect to the bulk layer stacking; the only ambiguity concerns the position of the row in the $[\bar{1}10]$ direction as mentioned above. Technically this amounts to exchanging the Pt and Fe species on consecutive sites along the dense row: this was realized by optimization of the occupation factor on each site simultaneously.

C. (1×2) analysis neglecting chemical order in the $[\bar{1}10]$ direction

Neglecting chemical ordering along the dense $[\bar{1}10]$ rows amounts to the optimization of 16 parameters: nine geometrical parameters describing the lattice relaxations within the top five layers (see Fig. 5) and seven additional parameters allowing a different Pt concentration in each nonequivalent row. The geometrical parameters were the same ones as considered in a previous study of the reconstruction of the clean Pt(110) surface,[1] namely, the interlayer spacings d_1 to d_5, row pairing in even layers Δy_2, Δy_4 and buckling in odd layers $\Delta z_3, \Delta z_5$. The optimization of the 16 parameters proceeded in three steps.

(a) In a first step, keeping all concentrations including that of the bulk at 80% Pt, five geometrical parameters related to layers 1 to 3 were determined (column 1 of Table I). The best r factor was $R_{\mathrm{DE}}=0.44$, corresponding to only poor agreement.

(b) In a second set of iterations, step 2, the concentrations within the first three layers (four nonequivalent rows), d_2, d_3, and the buckling Δz_3 in layer 3, were then optimized (column 2 of Table I). Before optimizing further relaxations and concentrations in layers 4 and 5, we introduced chemical order in the layers below the fifth layer. The alternate stacking of bulk layers with 100% Pt and 60%, respectively, made it necessary to distinguish two different terminations illustrated in Fig. 2. Both possibilities have been extensively tested assuming various combinations of Pt concentrations within different rows in the first three layers. The termination A, with a mixed occupation in the top layer [see Fig. 2(a)] led to a drop in the r factor to $R_{\mathrm{DE}}=0.38$, while the termination B [Fig. 2(b)] produced a clearly worse agreement $R_{\mathrm{DE}}=0.47$.

(c) In the third step of the analysis, the remaining variables in layers 4 and 5 as well as the lateral displacements Δy_2 and Δy_4 were optimized, partly together with the previously adjusted parameters. In a first run, 12 parameters were optimized simultaneously, leading to an optimum r factor $R_{\mathrm{DE}}=0.36$. Start values were the geometrical parameters determined previously, a bulk layer

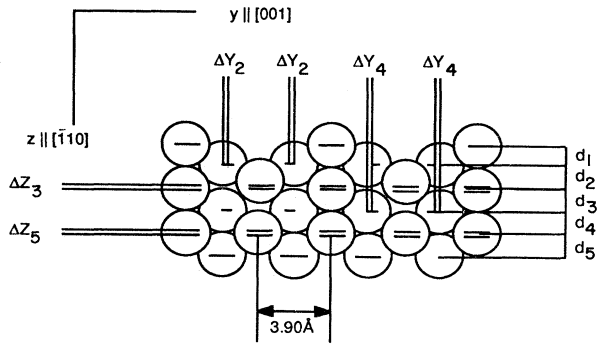

FIG. 5. Side view of the missing row model [(1×2) reconstruction], indicating the parameters optimized in the structure analysis.

TABLE I. Optimization omitting chemical order in the [$\bar{1}$10] direction; optimum parameters at various steps. All interlayer spacings given with reference to the center-of-mass plane. $d_{bulk} = 1.379$ Å.

	$\theta = 0°$				
			Step 3		
(Å)	Step 1	Step 2	Part 1	Part 2	$\theta = 20°$
d_1	1.18	1.18, fix	1.192	1.192,fix	1.189
d_2	1.33	1.33	1.321	1.321,fix	1.325
d_3	1.32	1.31	1.322	1.322,fix	1.323
d_4	d_{bulk},fix	d_{bulk},fix	1.384	1.384,fix	1.373
d_5	d_{bulk},fix	d_{bulk},fix	1.373	1.373,fix	1.376
ΔY_2	0.03	0.03,fix	0,fix	0.015	0.03, fix
ΔY_4	0,fix	0,fix	0,fix	0.01	0.01, fix
$\Delta Z3$	0.19	0.184	0.144	0.144,fix	0.151
$\Delta Z5$			0.052	0.065	0.060
(at. % Pt)					
$C_{1,1}$	80,fix	94	84	84,fix	84
C_2	80,fix	79	87	87,fix	82
$C_{3,1} = C_{3,2}$	80,fix	63	51	51,fix	51
$C_{3,3} = C_{3,4}$	80,fix	100	96	96,fix	96
C_4	80,fix	80,fix	82	82,fix	94
$C_{5,1} = C_{5,2}$	80,fix	80,fix	60,fix	60	57
$C_{5,3} = C_{5,4}$	80,fix	80,fix	60,fix	47	50
C_6	80,fix	80,fix	100,fix	100,fix	100,fix
$C_{7,1} = C_{7,2}$	80,fix	80,fix	60,fix	60,fix	60,fix
$C_{7,3} = C_{7,4}$	80,fix	80,fix	60,fix	60,fix	60,fix
Best R_{DE}	0.44	0.40	0.353	0.36	0.384

stacking corresponding to termination A starting at layer 6 and an overall Pt concentration of 80% in the three outermost layers. A minimum in the r factor was reached after 11 iterations. Finally, the lateral displacement and the concentration in the fifth layer were added. The latter parameters have little influence on the $I(V)$ curves and do not change the r factor significantly. Final values are presented in columns 3 and 4 of Table I.

A first important comment: the determined atomic positions, including (columns 3 and 4) or neglecting (columns 1 and 2) the chemical order in substrate layers, are very close to the final values of step 3. This clearly demonstrates that both sets of parameters—geometry and composition—are nearly uncorrelated. The slight change in the buckling in layer 3, from 0.19 to 0.15 Å is mainly caused by the fact that a buckling in layer 5 was not considered in the first step.

The second data set at oblique incidence, $\theta = 20°$ in the [$\bar{1}$10] azimuth, was used in an independent analysis because the current version of the program does not allow simultaneous optimization of experimental data sets at two different angles of incidence. The optimum parameters as determined previously were taken as start parameters and it was confirmed by simultaneous fit of 14 parameters that the minimum was reached (two variables, the lateral displacements, could not be included in the fit procedure, because the program does not allow a coupling of symmetrically equivalent positions). The final result was reached in three iteration steps with marginal changes of the parameters and similar agreement as that found for normal incidence as assessed by R_{DE} (=0.38). The values are shown in the last column of Table I.

That the *true minimum* was reached, and not a local minimum in the parameter space, was tested by choosing different start values for several parameters confirming that, again, the same minimum was reached. It was found that the geometrical parameters need to be about 0.02 Å within the minimum. This was done for different concentrations as well as for geometrical parameters. For instance, starting with a missing row model with all atoms at bulk lattice positions led to no improvement and R_{DE} above 0.8. Consequently, a contraction of the top layer spacing and a buckling in the third layer similar to that present in clean Pt(110)-(1×2) were assumed in the very beginning of the analysis. Conversely, for the layer concentrations, in most cases only one minimum existed in the total range from 0% to 100%. This is quite consistent with our findings relative to all unreconstructed alloy surfaces for which the minimum is unique.

It is particularly remarkable that the analysis of two independent data sets led to *nearly identical results.* All parameters deviate much less than the error limits: less than 0.01 Å for atomic distances and 5% for the rows Pt concentration. A bigger discrepancy (12%) is seen for the concentration of the fourth layer (C_4) only.

In an additional check, it was proven that the missing row model could be deduced from the optimization procedure. Starting with a pure Fe row in the position of the missing row, consistent with our finding of the termination A, and all other atoms at their optimized positions,

the Fe concentration in this particular row was optimized: R_{DE} dropped from 0.8 at 90 at. % Fe initially to 0.36 at 0% Fe after nine iterations, indicating clearly that *the missing row model is the correct picture.*

D. (1×2) analysis including chemical order in the [$\bar{1}$10] direction

The data set at normal incidence included five beams (h_0,k) reflecting the chemical ordering in the [$\bar{1}$10] direction. As mentioned above, although these beams have very small intensities, they carry the most significant information on the ordering along the dense rows. Consequently, we tried to optimize the additional parameters due to the twofold periodicity of the [$\bar{1}$10] rows.

In the termination *A* [Fig. 2(a)] there are five additional parameters describing the Pt site concentrations within the rows in layers 1, 3, and 5 (in layers 2 and 4, the four atoms/unit cell are symmetrically equivalent). Nonequivalent occupations of lattice sites also allow different geometrical parameters. Consequently, five additional *z* parameters have been considered whereas lateral displacements were neglected. Together with the 16 parameters of the (1×2) structure, this amounts to a total of 26 parameters within the top five layers.

In the first step, five beams only (71 data points at 15-eV steps) were used to optimize the concentration differences along the [$\bar{1}$10] direction, because only these beams reflect the chemical ordering along the rows. Different start values for concentration differences were used. In a final step, a simultaneous variation of all 26 parameters using all beams was performed proving that a minimum for all parameters had been reached. The results appear in column 3 of Table II compared to those of the optimum of the (1×2) analysis given in column 1. The sensitivity of R_{DE} (average over five beams) to chemical ordering in the top row was found to be quite high, nevertheless, no order was detected in layer 1. For instance, assuming a preferential occupation of 90% in site (1,1) and a depletion to 70% in site (1,2) led to a significant increase of R_{DE} to 0.42 from the minimum at 0.36. The top rows [sites (1,1) and (1,2)] happen to have an average concentration (82%) very close to that of the bulk. The geometrical parameters of the full analysis are displayed in Table III. The large number of parameters does not allow a conventional grid search with independent parameter variations. Therefore, only the search with the optimization procedure can be presented. To illustrate the reliability of the final results and to cross check the result by using conventional *r* factors, we performed full *I-V* curve calculations using a 3-eV step and varying some of the most significant parameters, i.e., the top three layer spacings and the site concentration in the third layer. All beams at normal incidence were used. Three different *r* factors, R_{DE}^{21}, R_P^{26} and R_{ZJ}^{27} as a function of one of the parameters are shown in Fig. 6 for all other parameters kept at their optimum values. Two *r* factors R_{DE} and R_P have very close values and, within the error limits, the same minima. R_{ZJ} seems to be less sensitive to the concentration changes. In all cases the minima agree with the minima located by the fit procedure using 15-eV steps indicated by the arrow in Fig. 6.

The sensitivity to site concentrations is in general much smaller than that to layer spacings. It has to be kept in mind, however, that a change in the concentration of a single site corresponds to a change in the average concentration by only a quarter. Obviously, larger error bars have to be assumed for the site concentrations and may be estimated to 20–30 % for a single site in the third layer.

TABLE II. Optimum concentrations when ordering in the [$\bar{1}$10] rows is considered via the limited data basis [five (h_0,k) beams], compared to the results obtained with disordered rows (average result from the two data sets). In odd layers atoms 1 and 2 (3 and 4), equivalent in the first analysis, become distinct in the presence of chemical order along the dense rows. Compare columns 1 and 4 (result from averaging over unequivalent sites).

Pt concentration (at. %)	Model with disordered rows (average over $\theta=0°+\theta=20°$) concentration	Truncated bulk concentration	Model with ordered rows atom[a]	Model with ordered rows average row concentration
$C_{1,1}$		20	82	
$C_{1,2}$	84	100	82	82
C_2	84	100	84	84
$C_{3,1}$		100	70–100	
$C_{3,2}$	51	20	0–20	48
$C_{3,3}$		100	80–100	
$C_{3,4}$	96	20	80–100	90
C_4	88	100	81	81
$C_{5,1}$		20	20–44	
$C_{5,2}$	59	100	80–100	61
$C_{5,3}$		20	5–20	
$C_{5,4}$	48	100	30–50	26
Best R_{DE}	0.36 0.38		0.36	

[a]See text.

TABLE III. $Pt_{80}Fe_{20}(110)(1\times2)$: atomic positions in the surface unit cell derived from the full analysis. Z positions are given with reference to the surface layer and with reference to the second bulk layer (no. 7). The last column displays the position corresponding to a truncated bulk. Bold figures denote atomic coordinates different from the expected bulk position.

Atom (layer, no.)	x (Å)	y (Å)	z (Å)	z' (Å)	z_{bulk} (Å)
1,1	0	0	0	**-8.18**	−8.28
1,2	2.76	0	0	**-8.18**	−8.28
2,1	1.38	**1.98**	**1.20**	**-6.98**	−6.90
3,1	0	0	**2.68**	**-5.50**	−5.52
3,2	2.76	0	**2.52**	**-5.66**	−5.52
3,3	0	3.90	**2.68**	**-5.50**	−5.52
3,4	2.76	3.90	**2.52**	**-5.66**	−5.52
4,1	1.38	**1.96**	**4.00**	**-4.18**	−4.14
5,1	0	0	**5.44**	**-2.74**	−2.76
5,2	2.76	0	**5.38**	**-2.80**	−2.76
5,3	0	3.90	**5.44**	**-2.74**	−2.76
5,4	2.76	3.90	**5.38**	**-2.80**	−2.76
6,1	1.38	1.95	−6.81	−1.38	−1.38
7,1	0	0	8.18	0	0
7,2	2.76	0	8.18	0	0
7,3	0	3.90	8.18	0	0
7,4	2.76	3.90	8.18	0	0

The sensitivity to chemical ordering in deeper layers was significant enough to conclude the following. (a) The buried row of layer 3 is ordered; atoms (3,1) and (3,2) have rather different concentrations whereas we systematically found the "visible" row of the same layer to be almost pure in Pt. (b) the contrast between unequivalent sites is still noticeable in the fifth layer. (c) No or almost no chemical contrast is seen along the rows in the even layers, those which are homogeneous in bulk. (d) On the contrary, with the striking exception of the first layer, the odd layers exhibit some contrast within the rows and those sites which should be Pt (Fe rich) atoms are actually occupied by Pt rich (Fe rich) averaged atoms. We restrict the final results to upper and lower limits for these parameters: the trends can be estimated as correct but one has to be prudent considering precise figures. (e) It is also worth mentioning that the average concentrations in the dense rows (last column of Table II) *reproduce almost perfectly* the figures derived from the (1×2) analysis (column 1).

The overall picture of the allow surface region is sketched in Fig. 7. For simplicity we have not distinguished the nonequivalent sites in the [$\bar{1}$10] direction, keeping the average concentrations of column 4 of Table II proposed as the final and safe result. In addition, we have used a limited grey scale to represent different levels of Pt concentration. Block, grey, and white circles denote 100%, 80%, and 60% Pt, respectively. Hatched circles correspond to a Pt concentration smaller than 60%. The interesting facts are the following.

(a) The topmost row (containing only 16% Fe) seems totally distorted.

(b) The ordering gradually recovers the bulk situation over five to six layers.

Perfect order has been assumed to start from layer 6 with 100% Pt concentration, and layer 7 with 100% at site 1 and 20% Pt at site 2, respectively.

The actual situation can be compared with that of a truncated bulk (Table II, column 2). Those sites which should be pure Pt in the bulk are found to be Pt rich in the present case and similarly with Fe rich sites. For instance $C_{3,1}\sim85\%$ and $C_{3,2}\sim15\%$ Pt are very close to 100% and 20% for the truncated bulk. The main exceptions concern the top layer where all sites contain 82% instead of 20% and 100% and layer 3 with 95% everywhere instead of 20% and 100%. The fact that the top row is mixed is consistent with the bulk stacking given in Table I with a pure Pt sixth layer.

It is possible that the bulk ordering has been overestimated and that it is distorted within a thicker surface region. However, optimization of ordering in deeper layers has not been tried because (i) the remaining discrepancies in the fit of the $I(V)$ curves certainly cannot be explained by a shortcoming of variable parameters; (ii) the computational effort does not seem to be justified; and (iii) the sensitivity to parameters in deeper layers becomes too small.

With preferential occupation of different lattice sites, the average position might change as well, due to a difference in bond length and atomic radii. These were not detectable within the error limits of the present analysis. The optimization procedure localized a slight buckling of ±0.01 Å [Z difference between sites (3,1) and (3,3)] in layer 3 and an even larger buckling of ±0.05 Å

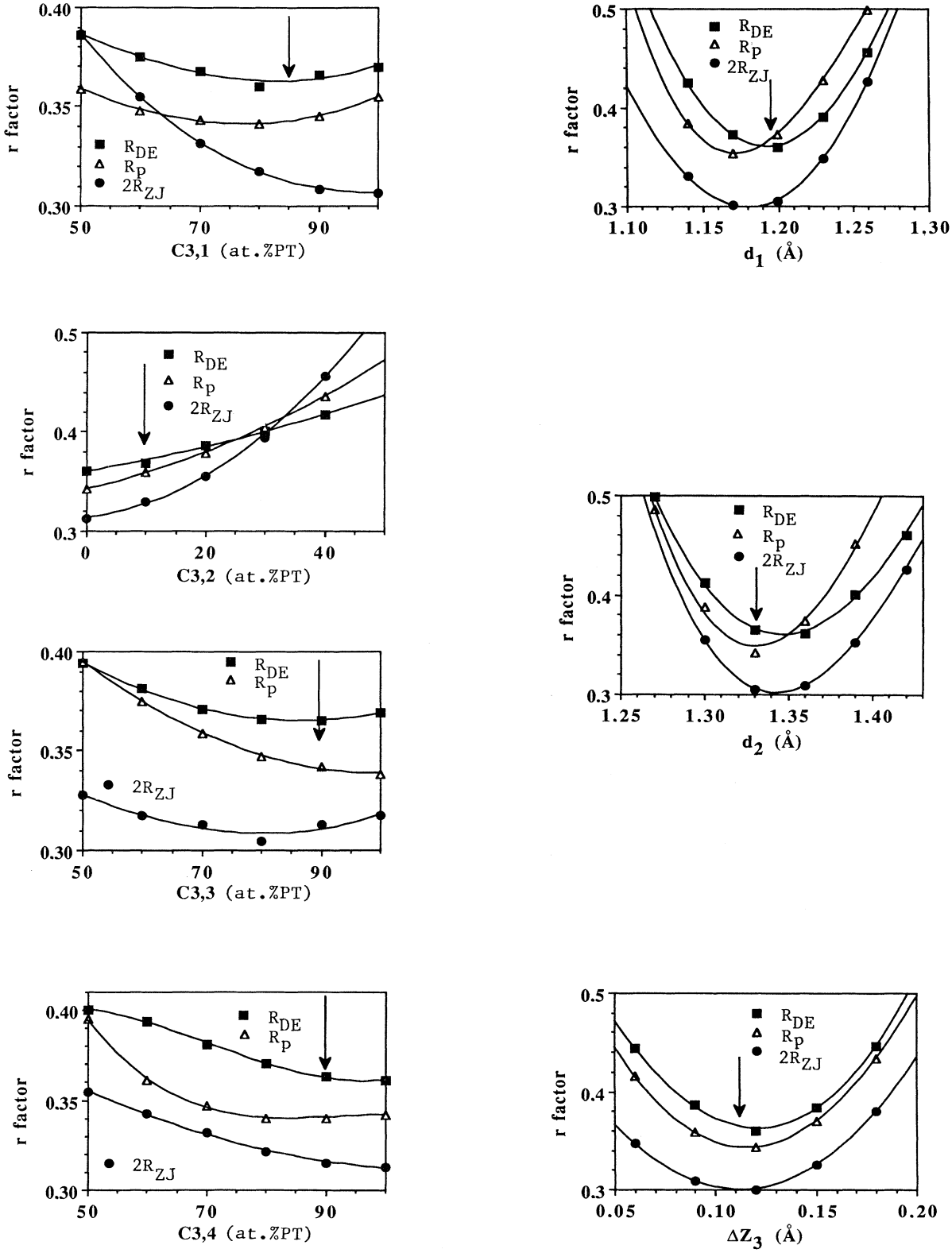

FIG. 6. Average r factors of 26 beams at normal incidence as a function of one parameter indicated in the figure, keeping all other parameters at their optimum value: Zanazzi and Jona's r factor (Ref. 26) (R_{ZJ}), and Pendry's r factor (Ref. 27) (R_P). For the calculations of the I-V curves, a step width of 3 eV was used. The arrows indicate the final result from the fit procedure using 15-eV steps (R_{DE}) (Ref. 21).

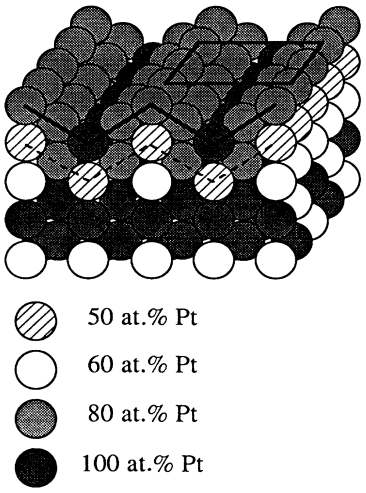

FIG. 7. $Pt_{80}Fe_{20}(110)(1\times2)$. Perspective view of the optimum structure showing schematically the average concentration in the different rows in layers 1 to 5. The missing rows are positioned with reference to the bulk layer stacking (last two layers) as revealed by the analysis. The surface region appears as a pile of corrugated layers enriched on the average, with Pt (——) and with Fe (— — —), respectively. Pt concentration is illustrated with an approximate grey scale. The chemical ordering along the [$\bar{1}$10] rows is not shown for the optimized surface layers.

[Z difference between sites (5,1) and (5,3)] in layer 5. Nevertheless, the data base with only five beams seems not to be sufficient to safely conclude about the existence of atomic displacement within the [$\bar{1}$10] rows.

The error bars may be estimated from the r-factor curves shown in Fig. 6. For the layer spacings and Z positions in the top three layers, a precision of 0.02 Å may be concluded. In the layers below the error bars are certainly larger, also the lateral positions have less influence on the I-V curves and consequently larger error bars. For the average concentrations, a limit of 5% can be accepted corresponding to about 20% for a single site concentration. Again, for the deeper layers, the sensitivity is smaller and the error bars may be larger. A more detailed discussion of the error bars seems not to be fruitful because of the unknown influence of systematic errors arising from the approximations in the calculations and because of the unknown reason of the remaining misfit.

VI. DISCUSSION

A. Structure analysis

The agreement between experiment and theory, although less good than for pure metals and/or simple unreconstructed surfaces, is similar to that obtained for the (1×2) reconstruction of pure platinum[1] or for the (2×2) reconstruction of the (111) face of the same alloy.[12] The r factor R_{DE} has a minimum value of 0.35 and 0.38 at normal and oblique incidence, respectively. This corresponds to the following values for other common misfit measures: $R_{Zj}=0.143$ (0.189), $R_P=0.34$ (0.363), and the metric distance[28] $D_1=18.1$ (19.6).

The quality of the experimental data cannot be questioned: very good accuracy is achieved in our goniometer for the angular setting, tilt adjustment of the crystal, and magnetic-field cancellation. It was carefully checked that equivalent beams produce the same spectra and that these spectra were reproducible. Moreover, the fact that two different data sets at different incidence angles yield the same geometrical optimum with a similar r-factor value is another indirect proof of the quality of the experiment (systematic errors would result in different answers).

Discrepancies due to the ATA approximation can similarly be discarded: the ATA approximation was certified in a number of analyses of binary compounds and successfully compared to CPA calculations on the one hand. On the other hand there are no possibilities left for further relaxations, segregation, bulk layer stacking, and ordering: all possibilities have already been investigated. It should be pointed out that the remaining misfit is too large to determine reliably all free parameters in the five top layers with the same precision. The main reason for including all free parameters within five layers was to exclude that any of these parameters is responsible for this misfit. The weak (h_0,k) beams exhibited a remarkable sensitivity to the concentration parameters in the fourth and fifth layers and possibly could be better fitted including further layers, but the response of the (h_e,k) beams to chemical ordering in deeper layers is small and the misfit could be explained by relaxation or concentration changes in deeper layers. It remains that the scattering potential calculated for bulk models might be not appropriate for the surface atoms: this seems to be unlikely because the scattering potentials were used in previous studied ending with excellent results.

One possible origin of the moderate agreement is in the treatment of thermal vibrations which were assumed isotropic in the present work. This might be concluded from the experience in structure analysis by x rays where low r factors and accurate geometrical parameters can only be reached after introducing anisotropic vibrations. There ia *a priori* no visible reason that this is different in the case of LEED. There are of course other approximations in the theory which might be responsible for the misfit, i.e., the muffin-tin approximation and the uniform damping. However, excellent results have been obtained for clean unreconstructed metals surfaces; but so far for none of the reconstructed (110) faces of Pt, Ir, or Au has better agreement been reached.

Though it seems unlikely that the defects in the surface alone are responsible for the misfit (diffuse intensities are too small), they might cause some disagreement. In particular, the reconstruction requires mass transport and the weak streaks observed in the LEED pattern indicate that defects are present in the surface. As can be seen from Fig. 8, mainly the high index beams exhibit considerable discrepancies between experiment and theory. This may be taken as a hint that disorder causes part of the remaining discrepancies as would be the case in a kinematic calculation.

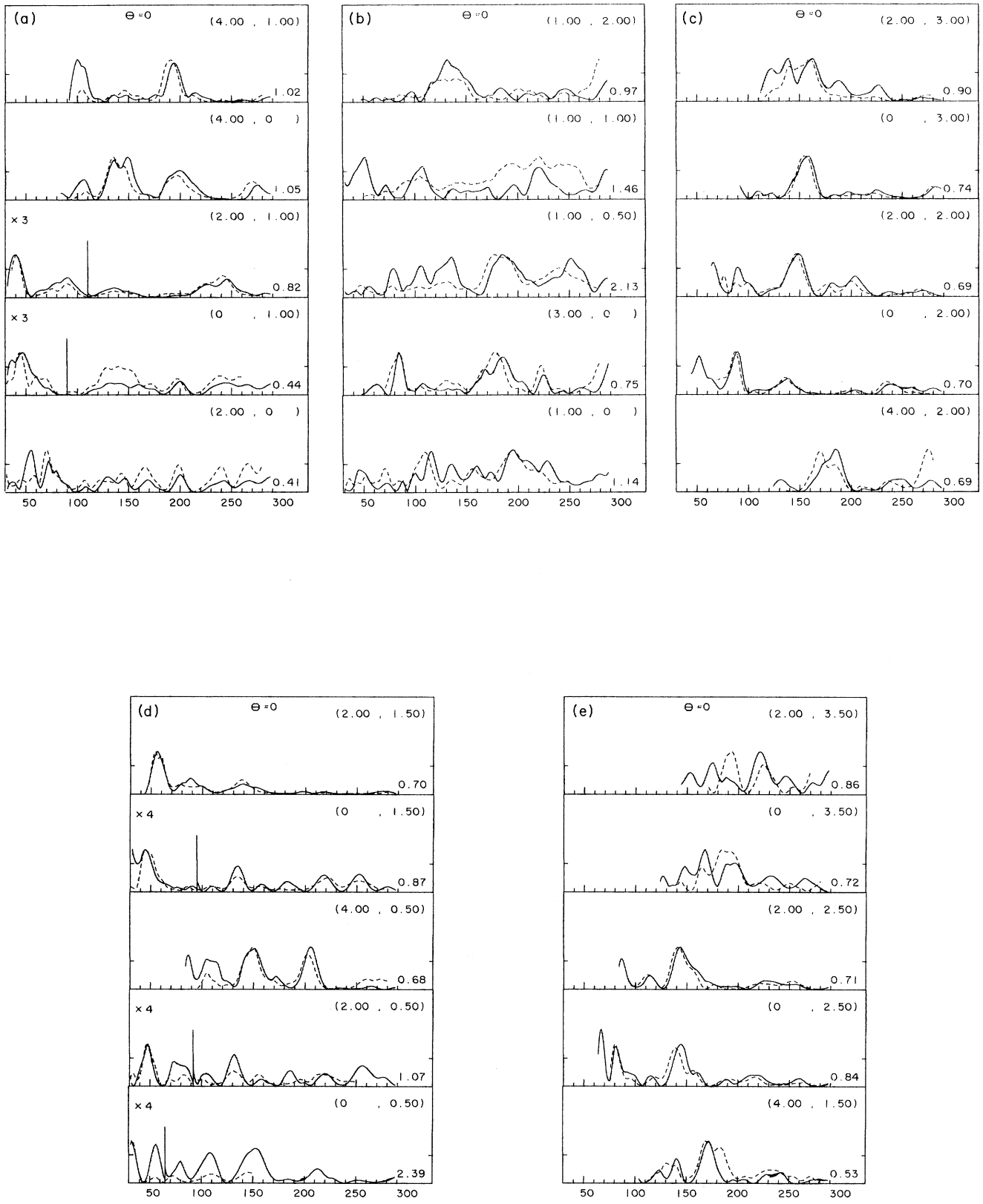

FIG. 8. $Pt_{80}Fe_{20}(110)(1\times2)$. Experimental (— — —) and calculated (——) $I(V)$ spectra. Concentrations and geometric parameters are those optimized with the overall data basis including chemical order in all layers (see Tables I and II).

B. Segregation and chemical ordering

The alloy selvedge can be viewed in two different ways.

(a) As a pile of flat (110) layers. In this picture, the top three layers show a bulklike Pt concentration; the third layer contains about 74% Pt, i.e., about the bulk content within the error limits.

(b) With missing rows, it can also be considered as a pile of "corrugated layers" constituted of the $[\bar{1}10]$ rows of layers numbered $i, i+1, i+2, i+1, i$ in sequence to form parts of (111) facets. Such layers are underlined in Fig. 6. The first corrugated layer—the surface available for adsorption—appears then as enriched with Pt with an average concentration of 87% while the second one underneath is depleted ($\sim$60%) in comparison with an equivalent bulk "layer" which contains 80%.

This would correspond to a Pt composition oscillation starting with Pt enrichment in the surface, in the fashion of that observed for the substitutionally disordered PtNi alloy, namely, Pt_xNi_{1-x} (111),[8,10] with $x=10-78$ %, and (110) (Ref. 17) or (100) (Ref. 18) surfaces with $x=10\%$. However, we do not observe the segregation reversal (oscillation + Ni enrichment in layer 1) found for $Pt_{50}Ni_{50}(110)$.[9]

Moreover, the $Pt_{80}Fe_{20}(110)$ face does not behave like the (111) face of the same alloy for which a monotonous decreasing Pt concentration was discovered.[12] In this latter case, the top layer contains 100 at. % Pt and one atom out of four in the unit cell is lifted up by 0.1 Å. No (111)-type ordering is found on the (111) facets of the corrugated layer but this may be due to too small facets. A more striking difference with disordered alloys lies in the fact that no chemical ordering is present in the (111) facets. In the case of $Pt_{10}Ni_{90}(110)$, (111), and (100), for instance, short-range chemical order in the very surface is assessed by the presence of extra features in the elastic background: Pt sites tend to be surrounded by Ni atoms. In the present case, with 82% Pt in the top row and 80–100 % Pt in the row down the valley, there is almost no possibility for such ordering. In summary, the present ordered bulk is topped with a disordered surface layer contrarily to the previously studied disordered alloys on top of which partial 2D ordering occurs.

C. Comparison with Pt(110)

As stated in Sec. III, there is a marked resemblance between pure Pt(110) and the alloy $I(V)$ spectra; it is highly interesting to compare the structural arrangements and also to quantify the differences. The comparison between the eight experimental spectra shown in Fig. 4 (the only one in common) yields average r factors $R_P=0.414$ and $R_{zj}=0.148$ for an energy range of about 1500 eV. If, for the alloy, we now compare the experimental and theoretical spectra of the same eight beams, the r factors are, respectively, $R_P=0.278$ and $R_{Zj}=0.098$, i.e., much lower than just above. This reinforces the argument above (end of Sec. VI A) concerning the high index beams which do not appear in this comparison. In addition, it is convincing to observe that the experiment-theory agreement comes out better than the experiment-experiment agreement for structures having close connections as expected prior to the analysis.

TABLE IV. Structural model of $Pt_{80}Fe_{20}(110)(1\times2)$ compared to that of pure reconstructed Pt(110) (Ref. 12). Interlayer distances are related to the center-of-mass plane. Buckling ΔZ, full distance ($\pm 1/2\Delta Z$); lateral shift ΔY, amplitude (shift from bulk positions).

Distances (Å)	Pt(110)(1×2)	$Pt_{80}Fe_{20}(110)(1\times2)$
d_1	1.10(−20%)	1.20(−13%)
d_2	1.37	1.40
d_3	1.38	1.40
d_4	1.42	1.41
d_5	1.36	1.40
ΔZ_3	0.17	0.15
ΔZ_5	0.03	0.06
ΔY_2	0.04	0.03
ΔY_4	0.04	0.01
d_{bulk}	1.387	1.379

Regarding the geometry, the comparison is made in Table IV with the results of Fery, Moritz, and Wolf.[1] Qualitatively the picture is essentially the same but some quantitative differences are noted. Generally speaking, all interlayer spacings down to the fifth layer are larger for the alloy than for Pt (110) except for d_4. For both crystals, the first interlayer spacing d_1 is reduced with respect to d_{bulk} although less for the alloy (13%) than for the pure metal (20%). From layer 2 on the spacing is even a little larger than d_{bulk} for PtFe. These differences cannot be explained by the difference in the bulk spacing (0.01 Å more for Pt). Buckling and pairing are found in deep layers in the same direction but with somewhat smaller amplitude.

For binary compounds, the bulk structure is often fixed by the bigger species. In the present case, Pt atoms have a metallic radius of 1.375 Å compared to 1.24 Å for iron. The iron concentration acts as a small perturbation resulting in a very weak difference in the lattice parameter (0.5%). Owing to the similarity in atomic positions, it is likely that the origin of the (1×2) reconstruction (still not fully understood) is the same as for clean Pt(110). It can be inferred also that the segregation of iron to some different sites [mainly to the (3,1) atomic position] is a consequence of the reconstruction.

VII. CONCLUSIONS

LEED calculations have shown that the geometric arrangement of the (1×2) reconstructed $Pt_{80}Fe_{20}(110)$ surface reproduces that of pure reconstructed Pt(110). Segregation is found to occur at some specific sites but does not influence much the reconstruction: the same atomic displacements are observed although they are generally less pronounced than for Pt(110).

The missing row reconstruction generates (111) facets which contain only a few percent iron. Because of the Fe

rich burried row of the second layer, these Pt rich facets are expected to yield modified catalytic properties as opposed to that of pure Pt; this was actually observed for the $Pt_{80}Fe_{20}(111)$ surface.

Besides the conclusions about atomic arrangement and segregation, additional conclusions can be drawn. It must be stressed that the calculated *I-V* curves show a remarkable sensitivity to the chemical order down to the fifth layer and to some extent also in the layers below. More specifically it was possible to distinguish between the two different terminations. The other clear outcome is that a very consistent picture has been found including the chemical ordering *along* the dense rows which gradually decreases from the bulk to the surface and is influenced by the reconstruction. Our previous findings in the analysis of $Pt_{80}Fe_{20}(111)$ were confirmed: atomic structure and concentrations are weakly correlated parameters in the *I-V* analysis so that the order can be gradually introduced or even neglected in some instances without spoiling the conclusions. This is particularly interesting when there are many parameters to optimize.

Finally we wish to emphasize that very complex structures such as the present one, including reconstruction, segregation, and partial order, become within the reach of LEED providing a fit procedure is used together with large data bases.

ACKNOWLEDGMENTS

We are indebted to the Centre de Calcul Verctoriel pour la Recherche for support with computer time. This work is part of the scientific program conducted by the Groupement Surface Rhône-Alpes and the European Science Foundation Network for Surface Crystallography.

*Permanent address: Institut für Kristallographie und Mineralogie, Univesität München, Theresienstrasse 41, 8000 München 2, Germany.

[1]P. Fery, W. Moritz, and D. Wolf, Phys. Rev. B **38**, 7275 (1988).
[2]W. Moritz and D. Wolf, Surf. Sci. **163**, L655 (1985).
[3]C. M. Chan and M. A. Van Hove, Surf. Sci. **171**, 226 (1988).
[4]W. Moritz and D. Wolf, Surf. Sci. **88**, L29 (1979).
[5]K. Christmann and G. Ertl, Z. Naturforsch. **28a**, 1144 (1973).
[6]M. Salmeron and G. A. Somorjai, Surf. Sci. **91**, 373 (1980).
[7]Y. Gauthier and R. Baudoing, in *Segregation and Related Phenomena,* edited by P. Dowben and A. Miller (CRC, Boca Raton, FL, 1990).
[8]Y. Gauthier, Y. Joly, R. Baudoing, and J. Rundgren, Phys. Rev. B **31**, 6216 (1985).
[9]Y. Gauthier, R. Baudoing, M. Lundberg, and J. Rundgren, Phys. Rev. B **35**, 7867 (1987).
[10]Y. Gauthier, R. Baudoing, and J. Jupille, Phys. Rev. B **40**, 1500 (1989).
[11]E. Goupil, P. Fouilloux, and R. Maurel, React. Kinet. Catal. Lett. **35**, 185 (1987).
[12]P. Beccat, Y. Gauthier, and R. Baudoing, Surf. Sci. **238**, 105 (1990).
[13]J. C. Bertolini (private communication).
[14]R. Hultgren, P. D. Desai, D. T. Hawkins, M. Gleiser, and K. K. Kelley, *Selected Values of the Thermodynamic Properties of Binary Alloys* (American Society for Metals, Metals Park, OH, 1973).
[15]W. B. Pearson, *A Handbook of Lattice Spacings and Structures of Metals and Alloys* (Pergamon, London, 1964).
[16]R. Baudoing and Y. Gauthier (unpublished).
[17]R. Baudoing, Y. Gauthier, M. Lundberg, and J. Rundgren, J. Phys. C **19**, 2825 (1986).
[18]Y. Gauthier, W. Hoffmann, and M. Wittig, Surf. Sci. **233**, 239 (1990).
[19]Y. Gauthier, Y. Joly, J. Rundgren, L. Johansson, and P. Wincott, Phys. Rev. B **42**, 9328 (1990).
[20]S. Crampin and P. J. Rous, Surf. Sci. **244**, L137 (1991).
[21]G. Kleinle, W. Moritz, D. L. Adams, and G. Ertl, Surf. Sci. **219**, L637 (1989).
[22]G. Kleinle, W. Moritz, and G. Ertl, Surf. Sci. **238**, 119 (1990); W. Moritz, H. Over, G. Kleinle, and G. Ertl, *Proceedings of the ICSOS Conference, Milwaukee,* (Springer-Verlag, Berlin, 1990).
[23]D. W. Marquardt, J. Soc. Ind. App. Math. **11**, 431 (1963).
[24]L. Clarke, Surf. Sci. **80**, 32 (1979).
[25]L. Clarke, R. Baudoing, and Y. Gauthier, J. Phys. C **15**, 3249 (1982).
[26]E. Zanazzi and F. Jona, Surf. Sci. **62**, 61 (1977).
[27]J. B. Pendry, J. Phys. C **13**, 937 (1980).
[28]J. Philip and J. Rundgren, in *Determination of Surface Structure by LEED,* edited by P. M. Marcus and F. Jona (Plenum, New York, 1984).
[29]W. Moritz, J. Phys. C **17**, 353 (1984).